PCCP

Accepted Manuscript

ROYAL SOCIETY OF CHEMISTRY

www.rsc.org/pccp

Colorimetric plasmon sensor with multilayered metallic nanoparticle sheets

Shuhei Shinohara, Daisuke Tanaka, Koichi Okamoto, Kaoru Tamada*

Institute for Materials Chemistry and Engineering & Department of chemistry, Kyushu University, Motooka Nishi-ku Fukuoka, 819-0395, Japan

E-mail:tamada@ms.ifoc.kyushu-u.ac.jp; Tel: +81-92-802-6230

Abstract

Colorimetric plasmon sensors for naked-eye detection of molecular recognition events are proposed. Here, 3-layered Ag nanoparticle (NP) sheets on an Au substrate fabricated by the Langmuir-Schaefer method were utilized as the detection substrate. A drastic color change was observed following the binding of Au NPs via the avidin-biotin interaction at less than 30% surface coverage. The color change was attributed not only to the localized surface plasmon resonance (LSPR) of the adsorbed Au NPs but also to the multiple light trapping effect derived from the stratified Au and Ag NPs, as predicted by a finite-difference time-domain (FDTD) simulation. This plasmonic multi-color has great potential in the development of simple and highly sensitive diagnostic systems.

1. Introduction

Simple, rapid and highly sensitive detection methods for biomolecules, such as viruses, pathogens and toxins, have been desired to realize a secure and reliable society.[1-4] Simple and inexpensive diagnostic systems that can be used for the home monitoring of diseases are also anticipated to support home healthcare and medical treatment. The most commonly used biosensing techniques are fluorescence immunoassay,[5] enzyme-linked immunosorbent assay (ELISA),[6] or their combined techniques. Surface plasmon resonance (SPR) and quartz crystal microbalance (QCM) sensors have also been developed as an alternative, label-free technique.[7-11] Recently, nanomaterials such as quantum dots and metallic nanoparticles have been utilized in combination with the aforementioned techniques[12-17] to enhance the signal intensity and improve the reliability of the diagnostics. A state-of-the-art ELISA test also uses metal nanoparticles (NPs) for colorimetric detection; for example, a blue color for a positive result and a red color for a negative result.[18,19]

Colorimetric detection by the naked eye is certainly the most simple and convenient diagnostic method, especially when it does not require any complex optical or electric system.[20,21] Metallic NPs have a high potential as color makers because they exhibit different colors depending on their size, shape, and nature, according to localized surface plasmon resonance (LSPR).[22,23]

Several methods of using LSPR-originated color have been developed for biosensing. When a dilute solution of metallic NPs is used for detection, the change in color is attributed primarily to the change in the refractive index of the surrounding medium, *i.e.*, the adsorption of biomolecules such as proteins onto the surface of the NPs. This phenomenon is reasonably interpreted by Mie's theory;[24,25] however, the color change caused by such isolated particles is not so large and is therefore unsuitable for highly sensitive detection.[26-28]

The previously described colorimetric methods used metal NPs are based on the change in resonance wavelength due to three-dimensional (3D) aggregation of NPs, which gives a much greater color change.[29-32] The color change by aggregation is interpreted by the Maxwell-Garnett theory (effective medium approximations) as the most classic interpretation[25,33] whereas El-Sayed et al. have

2

proposed an empirical "plasmon ruler equation" based on their experimental data with (2D) metallic disk pairs that they fabricated by electron beam (EB) lithography.[34]

Authors of recent studies in plasmonics have employed finite-difference time-domain (FDTD) calculations to discuss the correlation between LSPR band shifts and interparticle distances.[35,36] Our group has also investigated the characteristics of 2D crystalline sheets composed of Ag nanoparticles fabricated by self-assembly by both experiments and FDTD simulations and revealed the large influence of domain size (number of particles participating in 2D aggregates) on the resonance wavelength shift and on the interparticle distance.[37]

Such color changes caused by particle aggregation have already been commercially used for biomedical assays. However, this technique suffers from two main problems. One issue is the non-quantitative nature of the detection technique; only the presence or absence of analytes, but not their actual concentrations, can be quantified. The size distribution of the aggregates is one of the factors that makes this technique non-quantitative. Another problem is particle concentration. For naked-eye detection, an enormous number of particles are needed to associate in the reaction cells, although the number of target molecules does not always need to be high, especially for an enzyme reaction.[36, 37]

In this study, we challenge the limit of visual detection with the smallest number of particles immobilized on a surface and with good reproducibility. This work is based on our original development of "plasmon full color" with layer-by-layer-structured Ag NP sheets with further improvement.[38] When Ag NP sheets fabricated by self-assembly at an air-water interface were transferred to an Au substrate via the Langmuir-Schaefer method, the LSPR peak shifted to longer wavelengths and the light extinction increased nonlinearly with the number of layers, resulting in a significant reflection color change on the metal substrates. This phenomenon was observed not only Ag NP sheets[38] but also for Au NP sheets and even for hetero-structured Ag and Au NP sheets.[39] layer-number-dependent color changes were reasonably interpreted by two effects: the enhanced plasmon coupling between the layered NPs derived from the irradiation of reflected light on the metal substrate (large red-shift), and the multiple light trapping effect in the stratified metamaterial films

3

(extinction increase, with slight red-shift). These phenomena were reasonably reproduced by an simulation.[38] For the case of hetero-structured Ag and Au NP sheets, we cannot expect the plasmon coupling unlike homo particle system; however, still can expect the enhanced light trapping, which results in the enhanced extinction signal and additional red-shift.[39] A similar phenomenon (but LSPR coupling) was observed on nanometer-thick Ge (a highly absorbing dielectric medium) on a metal substrate.[40]

To design highly sensitive colorimetric biosensors, we chose the system that exhibits the largest color change following adsorption of a few particles, *i.e.*, 3-layered Ag NP sheets on Au substrate as an initial surface, and monitored the color change induced by the adsorption of Au NPs. A biotin-avidin interaction is used as a model molecular recognition system.[33,41] The adsorption of biotin-capped Au NPs onto an avidin-covered surface is monitored by naked-eye visual inspection and by reflection UV spectroscopy. The number of Au NPs adsorbed onto the surface is determined by scanning electron microscopy (SEM) images and surface plasmon resonance (SPR) spectroscopy, and the correlation with the color change is discussed.

2. Experimental

2.1 Synthesis of metallic nanoparticles and fabrication of 2D sheets

Ag NPs capped with myristates (AgMy) were synthesized by thermal reduction, as described in a previous study.[42] The Ag core was approximately 5 nm in diameter. A 2D crystalline sheet composed of Ag nanoparticles was fabricated in a Langmuir-Blodgett (LB) trough (KSV Mini-trough 2000), where self-assembly of the NPs was achieved by the hydrophobic interaction between myristates when the NPs were spread at the air-water interface. The interparticle distance, which is determined by the myristate capping molecules, was 2 nm.[42] The AgMy NP sheet was transferred via the Langmuir-Schaefer (LS) method to a hydrophobized Au substrate with 1-dodecanethiol self-assembled monolayers (SAM) at a surface pressure of 15 mN m^{-1}. The 3-layered AgMy NP sheet was fabricated by repeating the previously described procedure.

Au NPs capped with oleylamine (AuOA) were synthesized according to the procedure reported in a previous study.[40] The average diameter of the Au NPs was approximately 10 nm. The 2D sheets composed of Au NPs were fabricated in the same manner as the Ag NP sheets using the LS method at a surface pressure 15 mN m^{-1}. The interparticle distance, which was governed by the oleylamine capping molecules, was 2 nm.

2.2 Fabrication of colorimetric plasmon biosensor

The 200 nm-thick Au substrate was prepared by vacuum deposition on glass coated with a 3-nm-thick Cr adhesion layer. The SiO_2 sputtered films with 20 nm-thicknesses were deposited onto the 3-layered Ag NP sheets for surface bio-functionalization.[43,44] The SiO_2 surface was reacted with (3-aminopropyl)triethoxysilane (APTES, Sigma-Aldrich) and biotin-poly(ethylene glycol)-carbonate-NHS (SUNBRIGHT BI-050TS, NOF, Tokyo).[43] Streptavidin (Jackson ImmunoResearch, USA) was then immobilized on the biotinized-PEG surface in a 0.5 μM-PBS buffer solution with an incubation time of 30 min. Streptavidin was also immobilized on a 200 nm-thick Au substrate via biotin-functionalized PEG-thiol (Code 41151-0895; LCC Engineering and Trading GmbH, Switzerland) for a comparative experiment.

The Au NPs capped with citrates (AuCA) were synthesized by the reduction of $HAuCl_4 \cdot 3H_2O$ (Sigma, 99.9%) with sodium citrate, as described in a previous study (Frens's method).[33] The Au core was approximately 24 nm in diameter. Biotin-functionalized PEG-thiol was introduced onto the surface of the AuCA NPs with approximately 10% surface coverage via an exchange reaction for 4 h at room temperature.[33]

Fig. 1 shows a schematic of the colorimetric plasmon biosensor. The color change induced by adsorption of biotin-capped AuCA NPs onto the avidin-covered surface is monitored by visual inspection (the data were collected as color pictures taken with a regular digital camera) and reflection UV spectroscopy (UV-1800, Shimadzu). The 200 nm-thick untreated Au substrate was used as a reference surface to obtain extinction spectra.

2.3 Determination of surface coverage with Au nanoparticles

For the quantitative analysis, the number of biotin-capped AuCA NPs adsorbed onto the avidin-covered 50 nm-thick Au surface was counted from SEM images collected on a HITACHI High-Technologies SU-8000 scanning electron microscope. The images on the 50 nm-thick Au substrate were collected because those on the SiO_2-covered 3-layered AgMy sheets were not sufficiently clear to allow the number of particles to be counted; this lack of clarity was due to the charging effect caused by the SiO_2 layer.

Surface plasmon resonance (SPR) measurements were also performed using the same 50 nm-thick Au substrate to determine the averaged dielectric function of the biotin-capped AuCA adsorbed layer. A Kretschmann-type SPR setup with a p-polarized He-Ne laser (λ = 632.8 nm, R-DEC, Japan) and a high-refractive-index prism (LaSFN9, Scott, n = 1.85) was utilized for the measurements.[44] The average dielectric function of the AuCA composite layer was determined from the SPR angle shift and was converted to the surface coverage of biotin-capped AuCA NPs via the Maxwell-Gernett (MG) theory.[33,40]

2.4 FDTD simulations of plasmon color

FDTD simulations were conducted using commercial software (Poynting for Optics, Fujitsu, Japan). A model of multilayered Ag and Au NP sheets was developed on the basis of the experimental system, *i.e.,* 5 nm-Ag NPs or 10 nm-Au NPs in a hexagonally packed structure with an interparticle distance of 2 nm. The distance in the vertical direction was set to 4 nm by assuming no interdigitation myristates. The periodic boundary condition was set in the X and Y directions, whereas an absorbing boundary condition was set in the Z direction. For these calculations, we used pulsed light composed a differential Gaussian function centered at 1.5 fs with a width of 0.5 fs, an intensity of 1 V/m, and a bandwidth of approximately 600 THz (500 nm wavelength). The dielectric function of Ag was approximated by the Drude formula using previously reported values.[45] The dielectric function of Au known to be difficult to describe with the simple Drude formula.[46] However, because the FDTD calculation becomes highly complicated and unstable with the Drude-Lorentz formula, we performed the FDTD simulations of Au using the Drude formula in the same manner described in the previous

report.[46] The FDTD simulation with this simplified model of Au is known to be still available at least for the wavelength range from 500 nm to 1000 nm.

3. Results and discussion

3.1 Color tests with an AuOA monolayer on 3-layered AgMy sheets

Fig. 2a shows the result of the color test with the AuOA monolayer deposited on a 20-nm SiO_2 covered 3-layered AgMy sheets on a 200 nm-thick Au substrate. The intensity of the LSPR band originating from AgMy (λ_{max} = 533 nm) slightly decreased without spectrum shift once a 20-nm thick SiO_2 layer was deposited on 3-layered AgMy sheets. The decrease in intensity of the AgMy peak is understood as a release of trapping light by the SiO_2 layer. Upon deposition of the AuOA monolayer, the LSPR band originating from AuOA sheet appeared at λ_{max} = 680 nm, whereas the intensity of the LSPR band originating from AgMy increased again with substantial red-shift (λ_{max} = 550 nm), suggesting the 'enhanced light trapping' by the deposition of AuOA sheets. The color change was clearly demonstrated in this test experiment.

Fig. 2b shows the results of the FDTD simulation of the layered film with a monolayer (1L) of AuOA. Although the LSPR band positions and the extinction intensities differ slightly (mostly because of the dielectric functions of the metal used in the calculations), the trends of the multilayered films were reproduced in the simulation. In Fig. 2b, the credibility of the data at the wavelength region shorter than 450-nm is not high, because of the uncertainty of dielectric function of Au described by the simple Drude formula[46]. Therefore, we conducted the FDTD simulation on Ag substrate as well to guarantee of reliability of our calculation, and obtained quite similar results to that on Au substrate. The influence of organic layer (biotinized-PEG and streptavidin) was also confirmed with a 10-nm organic layer (n = 1.45) on the SiO_2 layer in the FDTD simulation. The spectrum becomes slightly broadened by the organic layer, but not large influence we found on the light trapping property.

Thus, we confirmed that 3-layered Ag NP sheets on an Au substrate are quite suitable as a substrate for the highly sensitive colorimetric detection of a few adsorbed Au NPs in the following molecular recognition study.

3.2 Detection of biotin-avidin binding using the colorimetric biosensor

Fig. 3a demonstrates the visual detection of biotin-avidin interaction with 3-layered AgMy sheets as the sensing substrate (avidin/biotin-PEG-SiO$_2$/3-layered AgMy/Au substrate). The data are shown together with the reflection spectra. Here, the concentration of biotin-capped AuCA was varied from 20.6 µg/ml to 1.19 mg/ml to obtain various surface coverages of AuCA. The incubation time was 1 h for all of the investigated concentrations. Fig. 3b shows the same experiments performed on the Au substrate (avidin/biotin-PEG-thiol/Au substrate) for comparison.

Fig. 3a reveals a significant change in color and in the extinction spectra in response to the adsorption of Au nanoparticles, whereas very little change was observed in the case of the reference Au substrate shown in Fig. 3b. In Fig. 3a, as the concentration of biotin-capped AuCA was increased, the LSPR peak originating from AgMy at 500–550 nm increased in intensity and red-shifted with the long tail to the longer wavelength, although the intensity of the peak originating from AuCA at 650 nm (see the bump on the red solid spectrum line) was as low as that in Fig. 3b. These results imply that the number of adsorbed AuCA particles is low even in a 1.19 mg/ml solution (highest concentration), although long tails of the band originating from the AgMy sheet drastically increased the extinction at longer wavelengths. The color change from pink to purple on the surface of 3-layered AgMy sheets is also clear in Fig. 3a, unlike that on the Au substrate shown in Fig. 3b. The specific interaction between the avidin surface and the biotin-capped AuCA NPs was confirmed by the control experiment with AuCA NPs without biotin functionalization (no color change; available in supporting materials).

3.3 Estimation of surface coverage with gold nanoparticles

We estimated the surface coverage by the biotin-capped AuAC NPs from SEM images and SPR angular shift data, where the 50 nm-thick gold substrates were used in common. Prior to particle adsorption, the formation of biotin-SAM and the streptavidin layer were confirmed by SPR kinetics and angular scan measurements. In our previous study, we confirmed that the dispersibility of biotin-capped AuAC NPs in aqueous solution and that on substrate varied with the pH of the solution.[41] At pH 6.5, which we have used in all of our experiments, the biotin-capped AuAC NPs are

8

well dispersed in solution and on substrate by surface charges originating from ionized citrates remaining on the AuAC surface. Under these conditions, the surface coverage with biotin-capped AuCA NPs remained low (maximum of 30 %) and the adsorbed particles were sufficiently far apart that no plasmon coupling occurred between them.

Fig. 4 shows SEM images of immobilized biotin-capped AuCA NPs at different concentrations at pH 6.5 on avidin-covered Au substrates. The AuCA NPs are well dispersed on the surface as described above. We counted the number of Au NPs using the ImageJ software and estimated the surface coverage on the basis of an average NP diameter of 24 ± 2 nm.[33] The obtained surface coverages are stated as percentages in the individual images in Fig. 4 (the errors are indicated in Fig. 6).

Fig. 5 shows the SPR angular scan data for the same surface shown in the SEM images. The SPR curves shifted to larger angles with increasing solution concentration, indicating that the number of adsorbed biotin-capped AuCA NPs increased monotonically with the solution concentration. The SPR angular shifts were converted to the dielectric functions of the particle composite layers, where the thickness of the layer was assumed to be equal to the diameter of the AuCA NPs ($d = 24$ nm). The obtained dielectric functions are listed in Table 1.

The correlation between the real component of the effective dielectric constant of the particle composite layer (ε'_{eff}) at $\lambda = 632.8$ nm and the volume fraction f of the particles in the layer was calculated by the simplified Maxwell-Garnett equation (eq. 1) [33]:

$$\varepsilon'_{eff} = \varepsilon'_m + \frac{AC + BD}{C^2 + D^2} \qquad (1)$$

where $A \equiv f(\varepsilon' - \varepsilon'_m), B \equiv f\varepsilon'', C \equiv \varepsilon'_m + \beta(\varepsilon' - \varepsilon'_m) - f\gamma(\varepsilon' - \varepsilon'_m), D \equiv \beta\varepsilon'' = f\gamma\varepsilon'' - f\gamma(\varepsilon' - \varepsilon'_m)$ and γ is described as

$$\gamma = \frac{1}{3\varepsilon'_m} + \frac{K}{4\pi\varepsilon'_m} \qquad (2)$$

9

where ε' and ε'' are the real and imaginary parts of the dielectric function of Au NPs, respectively; we used the values obtained in our previous study, (–8.03, 3.33).[33,41] Parameter ε'_m is the dielectric function of the matrix phase, *i.e.*, water in our experiments. K represents the dielectric field at a particle position created by the adjusted particles and/or by the surrounding medium and is considered to be nearly zero for the isolated particles in our study. If $K = 0, \gamma$ becomes $1/(3\varepsilon'_m)$. β is a geometric factor and is equal to 1/3 for the spherical particles. From the ε'_{eff} value obtained from the SPR measurements and the correlation curve (available in the supporting materials), we estimated the volume fraction f of the adsorbed biotin-capped AuCA NPs and subsequently converted this fraction to surface coverage (area fraction). The obtained values are listed in Table 1. Here, we note that the SPR measurement on 3-layered AgMy sheet is not possible because of the sample's excessively high optical thickness (the resonance angle was observed over an 80-degree range of incident angles, even when a high-refractive-index LaSFN9 prism was used[44]).

Fig. 6 shows the correlation between the surface coverages of biotin-capped AuCA NPs on avidin-covered Au substrates, as estimated from the SEM images and the SPR angle shifts. The data show good linearity and confirm the reliability of our experiments.

3.4 Correlation between color change and surface coverage with Au NPs

Fig. 7 summarizes the correlations between the position and intensity of the extinction peak and the surface coverage with AuCA NPs. First, the peak originating from the AgMy sheets (λ = 500–550 nm) is analyzed. We note that the surface being characterized by SEM and AFM is not that with 3-layered AgMy sheets (Fig. 3a) but that without AgMy sheets (Fig. 3b); thus, relatively large errors should be considered likely on the X-axis. Even so, Fig. 7 shows almost linear correlations between the LSPR band position and the surface coverage (a) and between the LSPR band intensity and the surface coverage (b). It is noteworthy that only a few % of AuCA adsorption induces about 10 nm-LSPR band shift (see the Y-intercept in Fig. 7a), which is linearly red-shifted to the wavelength of 550 nm up to 30% surface coverage. The extinction intensity also increased from 1.2 to 2.0 by the

adsorption of AuCA. The extinction data show a linear correlation as well, although they are scattered unlike the LSPR wavelength. These phenomena were reasonably interpreted by the enhanced light trapping efficiency due to an adsorption of Au nanoparticles on top of multi-layered sensor device, as predicted by the FDTD simulation.

Fig. 8 shows a plot of the extinction intensity at 650 nm, which is the wavelength of the LSPR band originating from the Au NPs. Here the data on the 3-layered AgMy sheet was compared with those for on the Au substrate. The peak intensity was enhanced more than two fold, even in the region of low surface coverage (less than 10%). However, the extraordinary characteristics of this detection method appeared (consequently) at a slightly higher surface coverage region: 10-30%. The extinction intensity increased nonlinearly as the surface coverage increased, and a signal 10 times stronger was observed at 30% surface coverage. This phenomena is also attributed to the light trapping effect produced by the additional AuCA layer on avidin/biotin-PEG-SiO$_2$/3-layered AgMy/Au substrate. Because the extinction efficiency did not yet reach its saturated value, it continued to increase with increasing surface coverage.

A quantitative discussion of the limit of visual detection is difficult because of individual difference of ability for color discrimination; however, our spectrum data adequately demonstrate the future potential of this naked-eye detection method. The merit of our detection system compared with other conventional colorimetric sensor[29-32] is that we can obtain a color change by adsorption of very little amount of nanoparticles on solid substrates, and the reflection type color obtained is a brilliant metallic color, which can be easily recognized by human eyes. Our sensor does not need a macroscopic size of diagnostic assay chip (sensing station) and can be incorporated into ultra-small microfluidic system. Although we demonstrated the color change from pink to purple in this study, the color is flexibly tunable in a wide range by the appropriate combination of metallic NP sheets (metal spices, layer number, layer order, etc.) [38,39] according to a request of potential customers including color vision defectives. The fact that the simulation correctly reproduces the color before the experiments are conducted is another advantage of this technique.

11

4. Conclusions

In this study, the new idea of a colorimetric plasmon sensor composed of multilayered Ag NP sheets on Au substrates was proposed. The key advantages of this technology are as follows: i) the device can be fabricated by self-assembly (bottom-up nanotechnology) and is therefore inexpensive and environmentally friendly; ii) it does not require any complex optical or electric systems because the signals are detectable by the naked eye as a vivid metallic full-color immediately after reaction; iii) 2D detection can be a platform for high-density and high-throughput on-chip sensing devices in combination with µTAS or Lab on a Chip technologies (in practice, a sandwich assay with Au NP as a maker must be used); and iv) the system can be made more sensitive or unique by optimizing the design of the layered structure according to the target materials. This colorimetric plasmon sensor may have promising potential applications in the fields of clinical diagnosis, drug screening, toxin detection and so forth. In particular, it may have strong potential as a disposable chip for home healthcare.

Acknowledgements

Table 1 Surface coverage with biotin-capped AuCA NPs on an avidin-covered Au substrate against the concentration of biotin-capped AuCA solution, as estimated by SPR and SEM

Concentration	13.7 (µg/ml)	20.6 (µg/ml)	41.2 (µg/ml)	103 (µg/ml)	208 (µg/ml)	515 (µg/ml)	1.03 (mg/ml)	1.19 (mg/ml)
ε'_{eff}(*)	1.80	1.81	1.85	1.94	2.06	2.54	2.76	3.12
SPR (%)	0.90	1.20	2.10	4.65	7.95	19.35	24.15	31.5
SEM (%)	0.57	1.17	2.77	3.81	11.77	19.00	23.25	-

(*)Effective dielectric constant (real part) of the AuCA adsorbed layer (d = 24 nm), as determined by SPR measurement

References

1   P. Tallury, A. Malhotra, L. M. Byrne and S. Santra, *Adv. Drug Deliv. Rev.,* 2010, **62,** 424-437.

2   P. D. Skottrup, M. Nicolaisen and A. F. Justesen, *Biosens. Bioelectron.,* 2008, **24**, 339–348.

3   I. Palchetti and M. Mascini, *Anal. Bioanal. Chem.,* 2008, **391**, 455–471.

4   D. Ivnitski, I. Abdel-Hamid, P. Atanasov and E. Wilkins, *Biosens. Bioelectron.,* 1999, **14**, 599–624.

5   Alvydas J. Ozinskas, *Principles of Fluorescence Immunoassay, Kluwer Academic Publishers, Boston,* 1994, **4**, 449-496.

6   H. Buss, T. P. Chan, K. B. Sluis, N. M. Domigan and C. C. Winterbourn, *Free Radic. Biol. Med.,* 1997, **23**, 361–366.

7   S. Chen, M. Svedendahl, R. P. Van Duyne and M. Käll, *Nano Lett.,* 2011, **11**, 1826–1830.

8   J. Homola, *Anal. Bioanal. Chem.,* 2003, **377**, 528–539.

9   B. P. Nelson, T. E. Grimsrud, M. R. Liles, R. M. Goodman and R. M. Corn, *Anal. Chem.,* 2001, **73**, 1–7.

10   L. B. Sagle, L. K. Ruvuna, J. A. Ruemmele and R. P. Van Duyne, *Nanomedicine Lond.,* 2011, **6**, 1447–1462.

11   C. A. Keller and B. Kasemo, *Biophys. J.,* 1998, **75**, 1397–1402.

12   Y. Xia, J. Ye, K. Tan, J. Wang and G. Yang, *Anal. Chem.*, 2013, **85**, 6241–6247.

13   N. L. Rosi, and C. A.Mirkin, *Chem. Rev.,* 2005, **105**, 1547–1562.

14   M. Hu, J. Yan, Y. He, H. Lu, L. Weng, S. Song, C. Fan and L. Wang, *ACS Nano,* 2010, **4**, 488–494.

15   A. Fornara, P. Johansson, K. Petersson, S. Gustafsson, J. Qin, E. Olsson, D. Ilver, A. Krozer, M. Muhammed and C. Johansson, *Nano Lett.,* 2008, **8**, 3423–3248.

16   M. A. Hahn, J. S. Tabb and T. D. Krauss, *Anal. Chem.,* 2005, **77**, 4861–4869.

17   C. Zhang and J. Hu, *Anal. Chem.,* 2010, **82**, 1921–1927.

18   R. de la Rica and M. M. Stevens, *Nat. Nanotechnol.,* 2012, **7**, 821–824.

19   I. Willner, R. Baron and B. Willner, *Adv. Mater.,* 2006, **18**, 1109–1120.

20   A. R. Ferhan, L. Guo, X. Zhou, P. Chen, S. Hong and D.-H. Kim, *Anal. Chem.,* 2013, **85**, 4094–4099.

21   R. Duan, B. Wang, T. Zhang, Z. Zhang, S. Xu, Z. Chen, X. Lou and F. Xia, *Anal. Chem.,* 2014, **86**, 9781–9785.

22   A. J. Haes and R. P. Van Duyne, *Anal. Bioanal. Chem.,* 2004, **379**, 920–930.

23   T. A. Taton, *Science.,* 2000, **289**, 1757–1760.

24   P. K. Jain, K. S. Lee, I. H. El-Sayed and M. A. El-Sayed, *J. Phys. Chem. B,* 2006, **110**, 7238–7248.

25   T. P. Sujit Kumar Ghosh, *Chem. Rev.* 2007, **11**, 4797–4862.

26   M. S. Han, A. K. R. Lytton-Jean, B.-K. Oh, J. Heo and C. A. Mirkin, *Angew. Chem. Int. Ed. Engl.,* 2006, **45**, 1807–1810.

27   C. A. Mirkin, R. L. Letsinger, R. C. Mucic and J. J. Storhoff, *Nature,* 1996, **382**, 607–609.

28   F. Xia, X. Zuo, R. Yang, Y. Xiao, D. Kang, A. Vallée-Bélisle, X. Gong, J. D. Yuen, B. B. Y. Hsu, A. J. Heeger and K. W. Plaxco, *Proc. Natl. Acad. Sci. U. S. A.,* 2010, **107**, 10837–10841.

29   W. Zhao, M. A. Brook and Y. Li, *Chembiochem,* 2008, **9**, 2363–2371.

30   X. Su and R. Kanjanawarut, *ACS Nano,* 2009, **3**, 2751–2759.

31   R. Kanjanawarut and X. Su, *Anal. Chem.,* 2009, **81**, 6122–6129.

32   S. Song, Y. Qin, Y. He, Q. Huang, C. Fan and H.-Y. Chen, *Chem. Soc. Rev.*, 2010, **39**,

      4234–4243.

33   X. Li, K. Tamada, A. Baba, W. Knoll and M. Hara, *J. Phys. Chem. B,* 2006, **110**, 15755–15762.

34   P. K. Jain, W. Huang and M. A. El-Sayed, *Nano Lett.,* 2007, **7**, 2080–2088.

35   J. Zhang, Y. Fu, M. H. Chowdhury and J. R. Lakowicz, *Nano Lett.,* 2007, **7**, 2101–2107.

36   M. Couture, Y. Liang, H.-P. Poirier Richard, R. Faid, W. Peng and J.-F. Masson, *Nanoscale,*

      2013, **5**, 12399–12408.

37   M. Toma, K. Toma, K. Michioka, Y. Ikezoe, D. Obara, K. Okamoto and K. Tamada, *Phys.*

      Chem. Chem. Phys., 2011, **13**, 7459–7566.

38   K. Okamoto, B. Lin, K. Imazu, A. Yoshida, K. Toma, M. Toma and K. Tamada, *Plasmonics*,

      2012, **8**, 581–590.

39   A. Yoshida, K. Imazu, X. Li, K. Okamoto and K. Tamada, *Langmuir,* 2012, **28**, 17153–17158.

40   M. A. Kats, R. Blanchard, P. Genevet and F. Capasso, *Nat. Mater.,* 2013, **12**, 20–24.

41   X. Li, K. Tamada, A. Baba and M. Hara, J. *Nanosci. Nanotechnol.,* 2009, **9**, 408–416.

42   C. D. Keum, N. Ishii, K. Michioka, P. Wulandari, K. Tamada, M. Furusawa and H. Fukushima,

      J. Nonlinear Opt. Phys. Mater., 2008, **17**, 131–142.

43   K. Tawa, X. Cui, K. Kintaka, J. Nishii and K. Morigaki, *J. Photochem. Photobiol. A Chem.,*

      2011, **221**, 261–267.

44   D. Tanaka, S. Shinohara, E. Usukura, P. Wang, K. Okamoto and K. Tamada, Jpn. *J. Appl.*

      Phys., 2014, **53**, 01AF01-07.

45   P. B. Johnson and R. W. Christy, *Phys. Rev. B,* 1972, **6**, 4370–4379.

46   A. Vial, A.-S. Grimault, D. Macías, D. Barchiesi and M. L. de la Chapelle, *Phys. Rev. B,* 2005,

71, 085416.

Figure caption

Fig. 1 Schematic of colorimetric plasmon sensor with multilayered metallic nanoparticle sheet.

Fig. 2 (a) UV-Vis spectra before and after the deposition of an AuOA monolayer (1L) on 20-nm SiO_2/3-layered AgMy/Au substrate (above) and their color change (below). (b) FDTD simulation results of 1L AuOA on 20-nm SiO_2/3-layered AgMy/Au substrate.

Fig. 3 UV-Vis spectra before and after adsorption of biotin-capped AuCA onto avidin/biotin-PEG-SiO_2/3-layered AgMy/Au substrate (a) and onto avidin/biotin-PEG-thiol/Au substrate (b).

Fig. 4 SEM images of biotin-capped AuCA immobilized on an avidin-covered Au surface.

Fig. 5 SPR angular shift induced by adsorption of biotin-capped AuCA NPs at different concentrations on an avidin-covered Au surface.

Fig. 6 Correlation between surface coverage of biotin-capped AuCA NPs on a surface, as estimated from SEM images and SPR angle shifts. The errors of X- and Y-axis originate from the distribution of the particle diameter.

Fig. 7 Extinction peak position (a) and intensity (b) of biotin-capped AuCA NPs adsorbed onto avidin/biotin-PEG-SiO_2/3-layered AgMy/Au substrate vs. surface coverage with AuCA NPs; the extinction intensity was measured in the 500-550-nm wavelength range. The doted lines are linear approximation determined from the data without 0% surface coverage.

Fig. 8 Correlation between surface coverage with biotin-capped Au NPs and the extinction intensity at a wavelength of 650 nm.
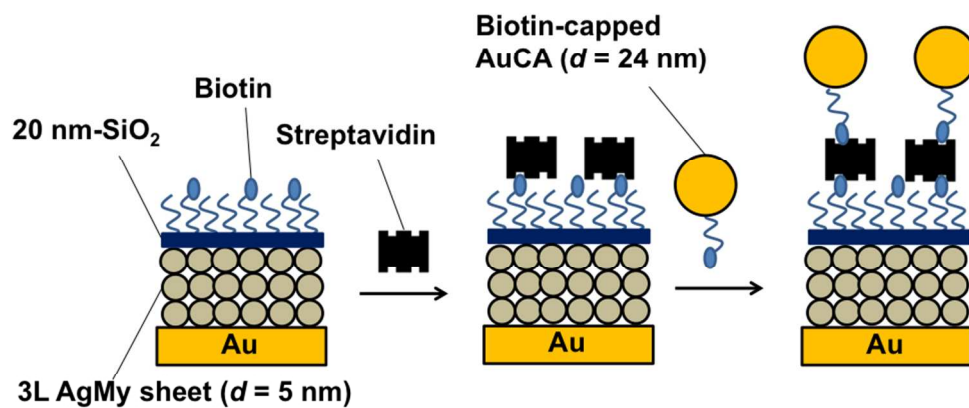
Schematic of colorimetric plasmon sensor with multilayered metallic nanoparticle sheet.
352x264mm (72 x 72 DPI)
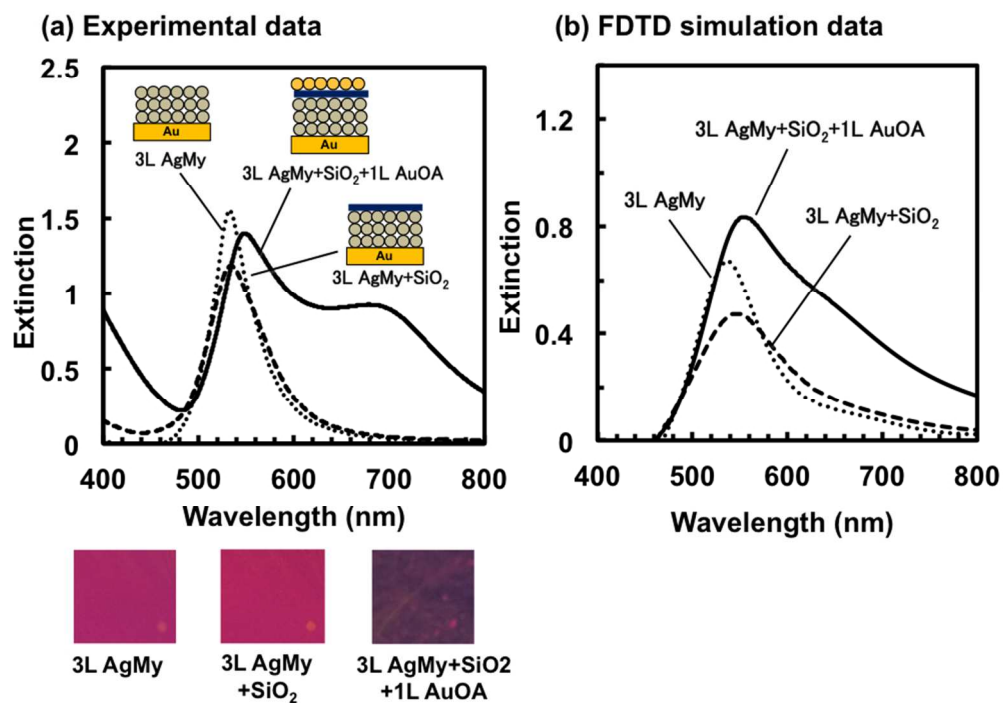
(a) UV-Vis spectra before and after the deposition of an AuOA monolayer (1L) on 20-nm SiO2/3-layered AgMy/Au substrate (above) and their color change (below). (b) FDTD simulation results of 1L AuOA on 20-nm SiO2/3-layered AgMy/Au substrate.

352x264mm (72 x 72 DPI)
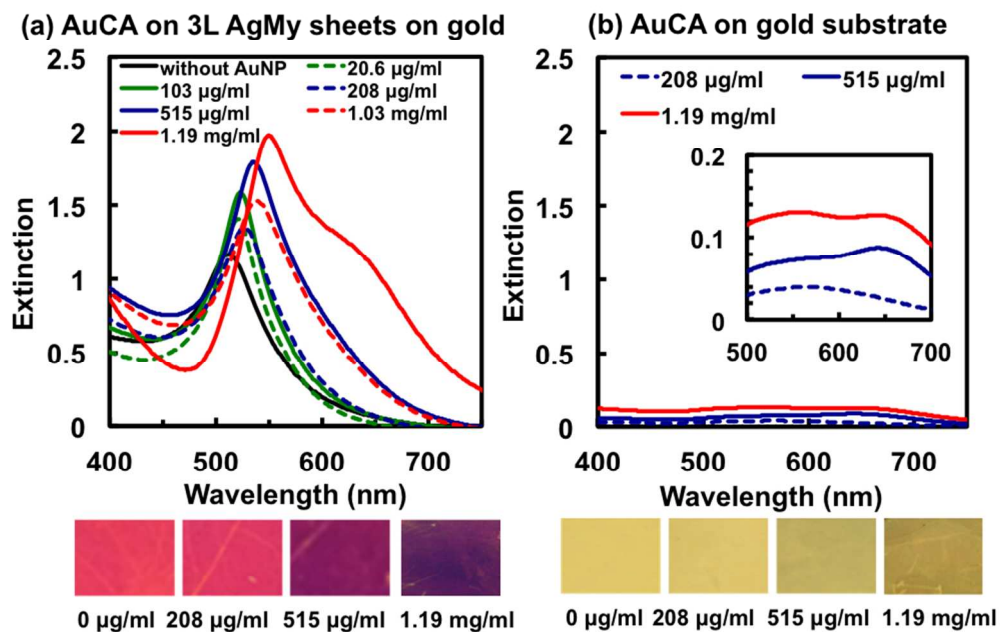
UV-Vis spectra before and after adsorption of biotin-capped AuCA onto avidin/biotin-PEG-SiO2/3-layered AgMy/Au substrate (a) and onto avidin/biotin-PEG-thiol/Au substrate (b).
352x264mm (72 x 72 DPI)
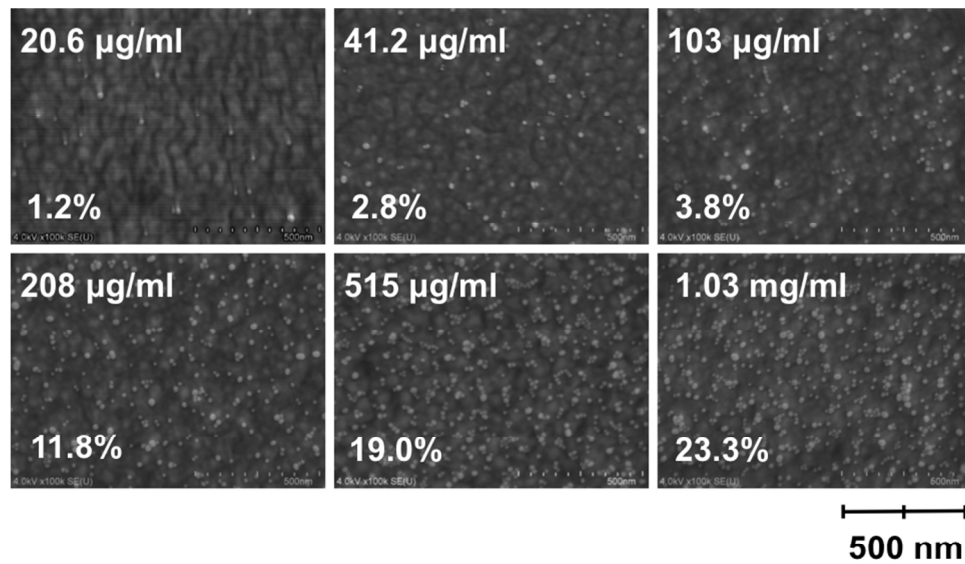
SEM images of biotin-capped AuCA immobilized on an avidin-covered Au surface.
352x264mm (72 x 72 DPI)
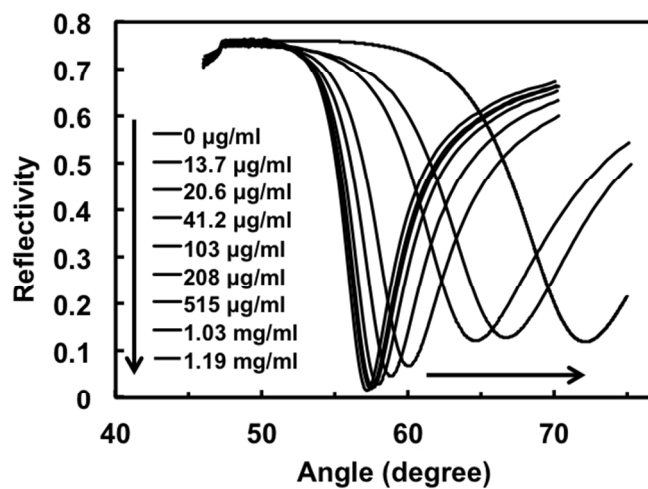
SPR angular shift induced by adsorption of biotin-capped AuCA NPs at different concentrations on an avidin-covered Au surface.

352x264mm (72 x 72 DPI)
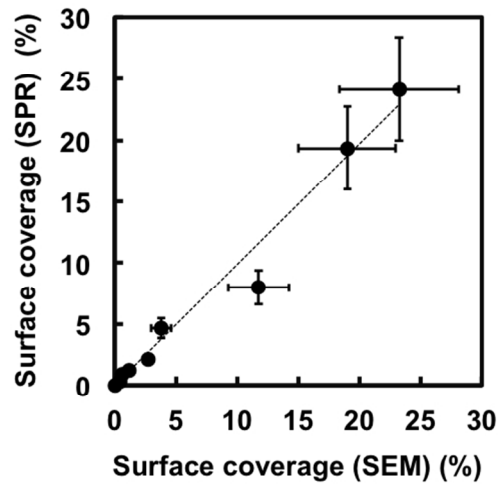
Correlation between surface coverage of biotin-capped AuCA NPs on a surface, as estimated from SEM images and SPR angle shifts. The errors of X- and Y-axis originate from the distribution of the particle diameter.
352x264mm (72 x 72 DPI)
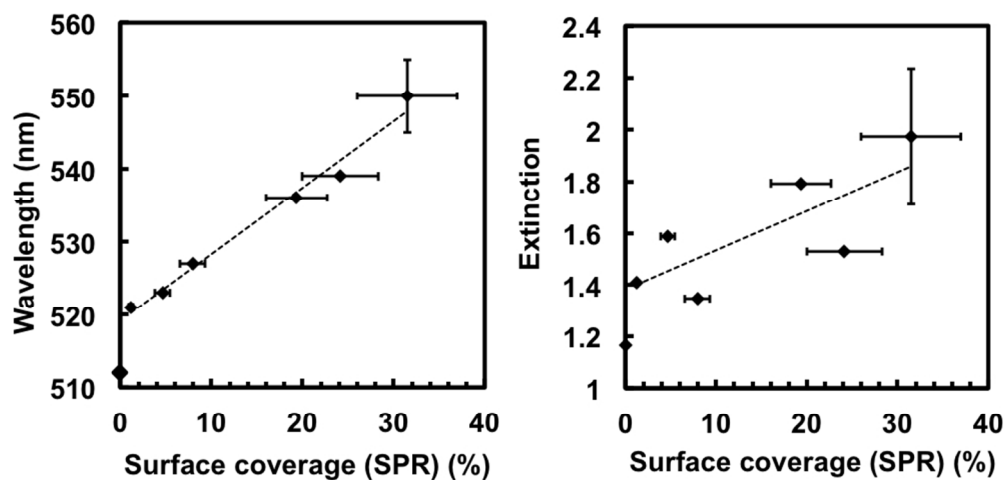
Extinction peak position (a) and intensity (b) of biotin-capped AuCA NPs adsorbed onto avidin/biotin-PEG-SiO2/3-layered AgMy/Au substrate vs. surface coverage with AuCA NPs; the extinction intensity was measured in the 500-550-nm wavelength range. The doted lines are linear approximation determined from the data without 0% surface coverage.
352x264mm (72 x 72 DPI)

352x264mm (72 x 72 DPI)